Cerebral Cortex, 2017; 1–14

doi: 10.1093/cercor/bhx136
Original Article

ORIGINAL ARTICLE

Neural Sources and Underlying Mechanisms of Neural Responses to Heartbeats, and their Role in Bodily Self-consciousness: An Intracranial EEG Study

Hyeong-Dong Park[1], Fosco Bernasconi[1], Roy Salomon[2], Catherine Tallon-Baudry[3], Laurent Spinelli[4], Margitta Seeck[4], Karl Schaller[5] and Olaf Blanke[1,6]

[1]Laboratory of Cognitive Neuroscience, Center for Neuroprosthetics and Brain Mind Institute, Ecole Polytechnique Fédérale de Lausanne (EPFL), 9 Chemin des Mines, 1202 Geneva, Switzerland, [2]Gonda Multidisciplinary Brain Research Center, Bar Ilan University, 52900 Ramat Gan, Israel, [3]Laboratoire de Neurosciences Cognitives (ENS – INSERM U960), Départment d'Etudes Cognitives, Ecole Normale Supérieure – PSL Research University, 75005 Paris, France, [4]Presurgical Epilepsy Evaluation Unit, Department of Neurology, Geneva University Hospital (HUG), 4 Rue Gabrielle-Perret-Gentil, 1205 Geneva, Switzerland, [5]Department of Neurosurgery, Geneva University Hospital (HUG), 4 Rue Gabrielle-Perret-Gentil, 1205 Geneva, Switzerland and [6]Department of Neurology, University of Geneva, 24 rue Micheli-du-Crest, 1211 Geneva, Switzerland

Address correspondence to Hyeong-Dong Park, Laboratory of Cognitive Neuroscience, Center for Neuroprosthetics and Brain Mind Institute, Ecole Polytechnique Fédérale de Lausanne (EPFL), 9 Chemin des Mines, 1202 Geneva, Switzerland. Email: hyeongdong.park@epfl.ch

Abstract

Recent research has shown that heartbeat-evoked potentials (HEPs), brain activity in response to heartbeats, are a useful neural measure for investigating the functional role of brain–body interactions in cognitive processes including self-consciousness. In 2 experiments, using intracranial electroencephalography (EEG), we investigated (1) the neural sources of HEPs, (2) the underlying mechanisms for HEP generation, and (3) the functional role of HEPs in bodily self-consciousness. In Experiment-1, we found that shortly after the heartbeat onset, phase distributions across single trials were significantly concentrated in 10% of the recording sites, mainly in the insula and the operculum, but also in other regions including the amygdala and fronto-temporal cortex. Such phase concentration was not accompanied by increased spectral power, and did not correlate with spectral power changes, suggesting that a phase resetting, rather than an additive "evoked potential" mechanism, underlies HEP generation. In Experiment-2, we further aimed to anatomically refine previous scalp EEG data that linked HEPs with bodily self-consciousness. We found that HEP modulations in the insula reflected an experimentally induced altered sense of self-identification. Collectively, these results provide novel and solid electrophysiological evidence on the neural sources and underlying mechanisms of HEPs, and their functional role in self-consciousness.

Key words: bodily self-consciousness, heartbeat-evoked potentials, insula, intertrial coherence, intracranial EEG

Introduction

There has been a recent resurgence of interest in brain–body interactions and their functional roles in cognitive and emotional processes (Craig 2009; Christoff et al. 2011; Critchley and Harrison 2013; Damasio and Carvalho 2013; Park and Tallon-Baudry 2014; Blanke et al. 2015; Garfinkel and Critchley 2016). Among internal organs, the heart has received much attention and neural representations of cardiac afferent signals have

been investigated by measuring heartbeat-evoked potentials (HEPs), which are obtained by averaging electrophysiological signals time-locked to heartbeats (Schandry et al. 1986; Pollatos and Schandry 2004; Gray et al. 2007). HEPs have been associated with various cognitive functions such as heartbeat awareness (Schandry et al. 1986; Montoya et al. 1993; Pollatos and Schandry 2004; Canales-Johnson et al. 2015), visual awareness (Park et al. 2014), self-consciousness (Babo-Rebelo, Richter, et al. 2016; Babo-Rebelo, Wolpert, et al. 2016; Park et al. 2016), self-face recognition (Sel et al. 2016), pain perception (Shao et al. 2011), empathy (Fukushima et al. 2011), sleep states (Lechinger et al. 2015), and psychiatric disorders including depression (Terhaar et al. 2012), depersonalization (Schulz et al. 2015), and borderline personality disorder (Muller et al. 2015). Most of these studies reported differential modulations of the HEP amplitude between different experimental conditions using scalp electroencephalography (EEG) or magnetoencephalography (MEG), to show the functional role of HEPs in the respective cognitive process. However, the basic properties (e.g., neural sources and the underlying electrophysiological mechanisms) of HEPs are not yet well understood. Thus, in the present study, we aimed to address 2 important questions regarding the fundamental properties of HEPs using intracranial EEG signals. What are the neural sources of HEPs? What is the underlying mechanism for the generation of HEPs? In addition, we also investigated the functional role of HEPs in bodily self-consciousness (Blanke et al. 2015; Park et al. 2016). More specifically, using intracranial EEG which has high spatiotemporal resolution, we aimed to replicate and anatomically refine our recent scalp EEG findings showing an association between HEPs and experimentally induced altered states of bodily self-consciousness (Park et al. 2016).

Regarding the neural sources of HEPs, although scalp EEG and MEG studies observed modulations of the HEP amplitude over frontal, central, and parietal channels in the time window from 200 to 650 ms post R-peak (for a review, see Kern et al. 2013), the involvement of specific physiological pathways underlying HEPs and their neural sources are so far poorly understood. For instance, previous studies reported that the amplitude of HEP is correlated with cardiac parameters such as cardiac output (Gray et al. 2007), and it has been proposed that mechanoreceptors in the heart wall and/or baroreceptors in the aortic arch may contribute to the HEP (Gray et al. 2007; Park et al. 2014). Animal studies suggested that such cardiac afferents are transmitted to cortical areas including the insula (Saper 2002; Craig 2003), amygdala (Cechetto and Calaresu 1985), somatosensory cortex (Dum et al. 2009) and cingulate cortex (Sikes et al. 2008), through subcortical relays such as the nucleus of the solitary tract, parabrachial nucleus, and thalamus (for a review, see Critchley and Harrison 2013). Source localization analysis using scalp EEG and MEG have also involved several brain regions and observed HEP modulations in the insula (Pollatos et al. 2005; Babo-Rebelo, Wolpert, et al. 2016), anterior/posterior cingulate regions (Pollatos et al. 2005; Park et al. 2014, 2016; Babo-Rebelo, Richter, et al. 2016), ventromedial prefrontal cortex (Park et al. 2014; Babo-Rebelo, Richter, et al. 2016), and somatosensory cortex (Pollatos et al. 2005). A recent intracranial EEG study (using subdural grid recordings) investigated the spatiotemporal distribution of HEPs (Kern et al. 2013) in 6 epileptic patients, and observed consistent HEP-like waveforms in the primary somatosensory cortex of 3 patients. However, this study had several limitations. First, neither statistical nor quantitative analyses were applied to prove the existence of such intracranial HEPs. Second, only signals recorded from grid electrodes positioned over the lateral cortical surface could be analyzed. This is an important limitation as the study did not record potential HEPs in the main viscerosensory and visceromotor regions: the insula, cingulate cortex, or amygdala (Craig 2009; Critchley and Harrison 2013; Damasio and Carvalho 2013; Park and Tallon-Baudry 2014). To overcome these limitations, in the present study, we analyzed 599 contacts from depth electrodes recorded from 8 epileptic patients using rigorous statistical procedures. Furthermore, we investigated the neural sources of HEPs by analyzing the intertrial coherence (ITC) of HEPs, which measures the degree of phase consistency over single trials at each electrode level (Tallon-Baudry et al. 1996). Increased ITC that is time-locked to heartbeats would provide strong electrophysiological evidence for the existence of HEPs, as it indicates that heartbeats induce consistent alignment of EEG waveforms across single trials.

Regarding the mechanisms of HEPs, 2 distinct electrophysiological mechanisms have been proposed for the generation of event-related potentials (ERPs): the phase-reset and the additive evoked potential model. According to the phase-reset model, ERPs are generated by a resetting of phases of ongoing oscillations in each single trial, whereas the evoked model proposes that stimulus-evoked responses in each single trial are added to generate the ERPs (Sauseng et al. 2007). ITC, combined with spectral power analysis, can provide critical information regarding the underlying mechanisms of ERP generation (Fell et al. 2004; Fuentemilla et al. 2006; Sauseng et al. 2007). For instance, the phase-reset model predicts that heartbeats will induce increased phase concentration over trials without an accompanying power enhancement, whereas the additive evoked model predicts that heartbeat-evoked spectral power will be enhanced (Shah et al. 2004; Sauseng et al. 2007). Although several studies have investigated the underlying mechanisms of sensory evoked brain potentials such as visual- and auditory-evoked potentials (Makeig et al. 2002; Rizzuto et al. 2003; Shah et al. 2004; Mazaheri and Jensen 2006; Rousselet et al. 2007; Lakatos et al. 2013), it is currently unknown which mechanisms underpin the generation of HEPs.

We further investigated the functional roles of HEPs in bodily self-consciousness (Blanke et al. 2015; Park et al. 2016). Several theories have proposed that interoceptive signals and their neural representations are critical for self-consciousness (Craig 2009; Christoff et al. 2011; Critchley and Harrison 2013; Damasio and Carvalho 2013; Park and Tallon-Baudry 2014; Blanke et al. 2015). In accordance with these theoretical proposals, using scalp EEG, we recently reported that modulations of HEPs recorded at frontocentral EEG channels were associated with altered states of bodily self-consciousness (Park et al. 2016). In that study, although dominant neural sources of HEP modulations were found in the posterior cingulate cortex, other sources might have contributed to the HEP effect but remained undetected due to the intrinsic limitations of source localization from scalp EEG data. Here, we focused our investigation on the insular cortex and the operculum which are considered to harbor the primary viscerosensory cortex and to be important regions for self-consciousness (Craig 2009; Critchley and Harrison 2013; Damasio and Carvalho 2013), as suggested also by recent lesion studies showed that damage to the insula is associated with abnormal states of bodily self-consciousness (Heydrich and Blanke 2013; Ronchi et al. 2015). Thus, from the original 8 epileptic patients, we recruited 4 patients and recorded intracranial EEG signals from the insula or the operculum while the patients participated in the well-established full-body illusion (FBI) paradigm (Lenggenhager et al. 2007; Ionta et al. 2011; Park et al. 2016) to experimentally alter bodily self-consciousness (Blanke et al. 2015).

Here, we show 3 main findings: (1) although HEPs are primarily observed in the insular and opercular regions, they are also found in other areas including the amygdala and frontal-temporal regions; (2) a phase resetting mechanism underlies HEP generation (Experiment-1); and (3) modulations of HEPs directly recorded at the insula are associated with an alteration of bodily self-consciousness (Experiment-2).

Materials and Methods

Patients

Intracranial EEG data were recorded from 8 epileptic patients (2 females, 2 left-handed, mean age: 32.4 ± 9.2 years; see Supplementary Table 1 for age, gender, handedness, epilepsy focus, heart rate, comorbidities, and medications of each patient) who were implanted stereotactically with depth electrodes for clinical purposes (i.e., presurgical evaluation for pharmacoresistant epilepsy). Among 8 patients, 2 were implanted with both surface grid electrodes (P-2:64 contacts; P-6:32 contacts) and depth electrodes. Surface grid electrodes from these 2 patients were not included in further data analysis because of low sample size of patients with such electrodes. All depth electrode recordings from all 8 patients were included, leading to a total of 599 depth electrodes from 8 patients that were analyzed in Experiment-1. Among these 8 patients, we specifically recruited 4 patients (P-1, P-2, P-5, P-8; 1 female, 1 left-handed, mean age: 27 ± 7.1 years) for the additional FBI experiment (Experiment-2, see below; Lenggenhager et al. 2007; Ionta et al. 2011; Park et al. 2016), as they were implanted with depth electrodes at the insular or operculum regions (P-1: bilateral, P-2: right hemisphere, P-5: left hemisphere, P-8: bilateral implantation) which are considered as the primary viscerosensory cortex (Craig 2003, 2009; Critchley and Harrison 2013). All patients signed a written informed consent, and all procedures were approved by the local ethics committee.

Experimental Procedure

In the main experiment (Experiment-1), we selected intracranial recordings that were obtained when the patients were awake and at rest (in bed) during presurgical epilepsy evaluation (mean recording time: 56.3 ± 10.6 min). Thus, there were not any specific experimental instructions for this period. The 4 patients participating in Experiment-2 were asked to perform the FBI task (Fig. 6), as fully described in our previous study (Park et al. 2016). In brief, the patients viewed an image of their own back in a sitting position through a head-mounted display (640 × 800 resolution, 110 degrees diagonal field of view) filmed from cameras (Logitech C510, Logitech) located 2 m behind, while the experimenter gave irregular stroking on their real back. During the synchronous condition patients viewed an image of their back in real-time, whereas 0.5 s of delay was introduced during the asynchronous condition. The patients performed 2 blocks of the FBI task, with one synchronous and one asynchronous block. At the end of each block, the patients were prompted to respond verbally to the questionnaire on self-identification to the viewed avatar (i.e., How strong was the feeling that the body you saw was you?) using a 7-point scale from 1 (bottom-extreme) to 7 (top-extreme).

Electrode Implantation, Intracranial EEG Recordings, and Preprocessing

In total, 599 depth contacts were implanted in 8 patients, covering diverse cortical and subcortical areas including the insula, operculum, amygdala, hippocampus, frontal and temporal cortex. All implantation sites were determined purely by clinical requirements. Three different types of electrodes were used for the recording: standard electrodes (66.8%, contact size: 2.4 mm, interelectrode spacing: 10 mm; e.g., Blanke et al. 2005), "short spacing" electrodes (23.9%, contact size: 1.32 mm, interelectrode spacing: 2.2 mm), and "micro" electrodes (9.3%, contact size: 1.6 mm, interelectrode spacing: 5.0 mm).

Intracranial EEG and electrocardiogram (ECG) signals were simultaneously recorded (Micromed System PLUS, Micromed, Mogliano Veneto, Italy) with a sampling rate of 2048 Hz, and online high-pass filtered at 0.02 Hz. The external reference electrode was located at position Cz (i.e., vertex). Continuous intracranial EEG data were down-sampled to 128 Hz and 512 Hz, respectively, for Experiment-1 and Experiment-2. A lower down-sampling rate was applied for Experiment-1, due to the excessive computational demand for the wavelet analysis applied to the large dataset (i.e., mean number of trials: 3346 ± 320; see below). In each patient, electrodes showing excessive noise (i.e., >3 SD; 49 electrodes in total) were excluded, and 550 clean contacts were used for further analysis. We computed bipolar signals by subtracting intracranial EEG signals of 2 adjacent electrodes (e.g., A1–A2, A2–A3…) from within each electrode shaft, to eliminate the influence of the common external reference and remote sources (Lachaux et al. 2003) including cardiac field artifacts (CFA) and pulse-related artifacts (PA) (Kern et al. 2013). In total, 474 bipolar derivations were obtained (mean number of bipolar derivations: 59 ± 11; Fig. 1). In Experiment-2, 41 bipolar derivations from depth electrodes which contained at least one insular or operculum recording site were analyzed (Fig. 7).

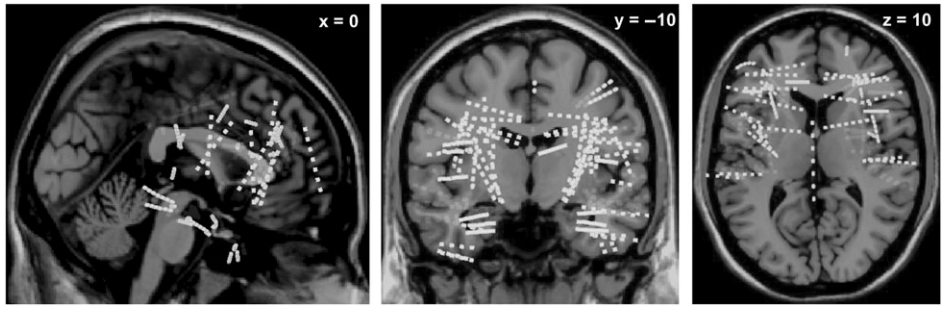

Figure 1. Locations of all recording sites in 3D MNI space. MNI coordinates of all bipolar derivations (i.e., midpoint between 2 contacts) from all 8 patients (474 bipolar derivations, $N = 8$) were computed and plotted on the Colin27 MRI template (sagittal, coronal, and axial planes). Note that locations are in 3D MNI space, and not located on the surface of MRI slice shown (thus, recording sites behind the depicted MRI slice are marked with faded color).

To compute the Montreal Neurological Institute (MNI) coordinates for each electrode, a postimplant computed tomography (CT) image was coregistered to the normalized preoperative magnetic resonance imaging (MRI) using Cartool Software (Brunet et al. 2011). A midpoint between 2 depth electrodes was considered as the location of the corresponding bipolar derivation. Then, locations of bipolar derivations were visualized on the Colin27 MRI brain template using the BrainStorm toolbox (Tadel et al. 2011). Anatomical description was based on the Harvard-Oxford cortical and subcortical structural atlases (Makris et al. 2006).

HEP Analysis

HEPs were computed on intracranial EEG signals locked to the R-peak of the ECG. We detected R-peaks on ECG by correlating ECG signal with a template QRS complex defined on a subject-by-subject basis, and identified local maxima within episodes of correlation larger than 0.7 (Park et al. 2014, 2016). For Experiment-1, epochs (−300 to 600 ms regarding the R-peak onset) showing excessive noise (i.e., >3 SD) were excluded from further analysis. After artifact correction, 3346 ± 320 epochs were averaged in each subject to compute HEPs. For Experiment-2, single epochs were visually inspected to confirm that no artifact remained. A total of 232 ± 62 and 229 ± 65 epochs were averaged, respectively, for synchronous and asynchronous stroking conditions.

ITC Analysis

Power and phase were calculated by using wavelet transform for the frequency range from 0.2 to 20 Hz in 0.2 Hz step. Frequency range was set in accordance with the previous studies that applied ITC analysis to ERPs, such as visual evoked potentials (Mazaheri and Jensen 2006), and auditory evoked potentials (Fuentemilla et al. 2006; see below for further justification on frequency band selection). Single trial data were convolved by a complex Morelt's wavelet: $w(t, f_0) = A \cdot \exp(-t^2/2\sigma_t^2) \cdot \exp(2i\pi f_0 t)$, using a constant ratio of $f_0/\sigma_f = 5$ where $\sigma_f = 1/2\pi\sigma_t$, and the normalization factor $A = (\sigma_t \sqrt{\pi})^{-1/2}$ (Tallon-Baudry et al. 1996). The degree of phase concentration across single trials were quantified by the ITC (Tallon-Baudry et al. 1996), which is defined as the average of normalized instantaneous phases over trials.

$$\mathrm{ITC}(f_0,t) = \frac{1}{N}\left|\sum_{k=1}^{N} e^{i\varphi k(f_0,t)}\right|$$

ITC values range between 0 and 1, with higher value indicating more consistent alignment of phases across single trials.

Importantly, in a previous study, it was shown that the waveforms of HEPs recorded from intracranial EEG are heavily contaminated by PA (Kern et al. 2013). Indeed, we also found that PA was the most dominant feature of the heartbeat-locked intracranial EEG signals in our data (Fig. 2A,B), even though bipolar referencing was applied. To dissociate ITC components reflecting HEPs from those reflecting PA, we excluded frequency bands that are lower than 4 Hz from further ITC analysis (Figs 3, 5 and 7). First, ITC components reflecting PA would be observed at the similar frequency band as the pulse or heart rate, which is normally lower than 2 Hz (see Fig. 2C). We confirmed that no patient had heart rate, obtained from randomly selected 10 min time window, faster than 1.33 Hz (see Supplementary Table 1). Second, we also wanted to remove higher order harmonics of PA (e.g., second and third order) that could be potentially observed in 2–4 Hz

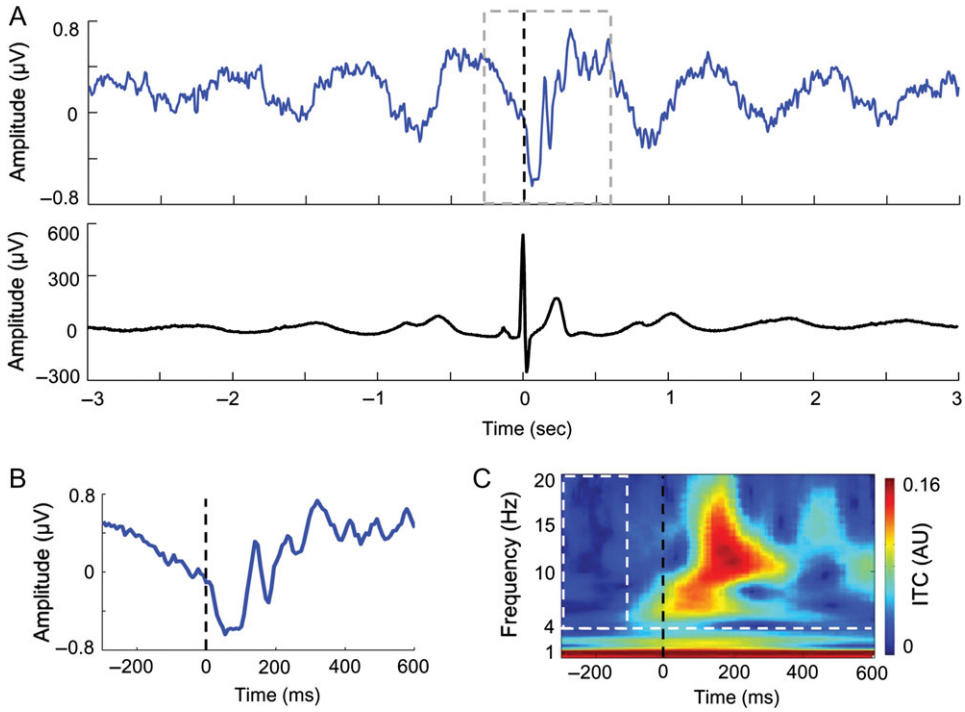

Figure 2. Rationale for analyzing ITC of HEPs. (*A*) An exemplar waveform of HEPs recorded at the insula (top) and ECG (bottom) in P-1, 6 s around the R-peak onset. (*B*) HEPs in the time window of interest (−300 to +600 ms regarding the R-peak onset), as marked in a gray dotted box in (*A*). (*C*) Time–frequency representations of ITC of HEPs that is shown in (*B*). White dotted horizontal line indicates threshold frequency (4 Hz) used to exclude low frequency pulse-related components whose main peak was observed around 1 Hz. A white dotted box indicates the time window used for the baseline correction. Note that no baseline correction was applied in this figure to show the original ITC values. Black dotted vertical lines indicate the onset of ECG R-peak.

frequency band (Norcia et al. 2015). Third, we hypothesized that phase modulation would be associated with ongoing theta (4–7 Hz), alpha (8–12 Hz), and low-beta (13–20 Hz) oscillations, based on previous studies investigated ITC modulation in sensory evoked potentials such as visual evoked potentials (Makeig et al. 2002) and auditory evoked potentials (Fuentemilla et al. 2006).

Furthermore, we also assumed that ITC components reflecting HEPs would transiently increase after the R-peak onset compared with the pre R-peak time window (Fig. 2C). Thus, the mean ITC value of the pre R-peak time window (−300 to −100 ms) was considered to be the baseline and was divided from the post R-peak ITC value in each frequency band (Fig. 3). We set such baseline (−300 to −100 ms) to avoid (1) smearing of post R-peak activity into the baseline (Roach and Mathalon 2008) and (2) a possible influence of cardiac artifact around ECG P-wave (Schandry et al. 1986).

Statistical Tests

In Experiment-1, to detect recording sites showing HEP components, we applied statistical tests for the results of the ITC analysis. Importantly, applying statistical tests on the averaged HEP waveforms could be misleading, as such test will be more sensitive for detecting PA components around 1 Hz which have a larger amplitude modulation (see Fig. 2). The significance of ITC enhancement was assessed using nonparametric permutation test complemented with the false discovery rate (FDR) correction procedure (Benjamini and Hochberg 1995; Groppe et al. 2011). For this, we created surrogate R-peaks that preserve the same interbeat interval (IBI) and variability with the original R-peaks, but randomly shifted in time (−500 to +500 ms regarding the original R-peaks) (Park et al. 2014, 2016). Then, for each time–frequency sample, ITC was computed following the same procedure used for the original data, separately in each electrode. Following this, the grand average of baseline corrected ITC across all the electrodes from 8 patients was obtained with the shuffled data. This procedure was repeated 1000 times, producing a distribution of the grand averaged ITC that could be observed by chance. For each sample, a *P*-value was obtained as the proportion of the grand averaged ITC from shuffled data that exceed the original grand averaged ITC. Then, we applied FDR procedure to *P*-values over all time–frequency samples to correct multiple comparisons (Benjamini and Hochberg 1995). A similar procedure was also applied in each electrode level, without averaging ITC values across all the recording sites.

In Experiment-2, the significance of differences of HEPs between synchronous and asynchronous conditions was tested using the cluster based permutation *t*-test (Maris and Oostenveld 2007) as implemented in the Fieldtrip toolbox (Oostenveld et al. 2011). In each subject, bipolar derivations from depth electrodes that contained at least one insular or opercular contact were analyzed (P-1:13 bipolar signals; P-2:7 bipolar signals; P-5:7 bipolar signals; P-8:14 bipolar signals). Two sample *t*-test was conducted between 2 conditions in each time point and in each recording site, and samples whose *t*-value exceeds a threshold ($P < 0.05$, two-tailed) are clustered based on temporal and spatial adjacency. Neighboring bipolar derivations in each depth electrode (e.g., A1–A2, A3–A4 for A2–A3) were considered as spatially adjacent. Each cluster defined in time and space by this procedure is assigned cluster-level statistics, corresponding to the sum of the *t*-values of the samples belonging to that cluster. Type-I error rate is controlled by evaluating the maximum cluster-level statistics under the null hypothesis: condition labels of trials were randomly shuffled 1000 times to estimate the distribution of maximal cluster-level statistics obtained by chance. The two-tailed Monte-Carlo *P*-value corresponds to the proportion of the elements in the distribution of shuffled maximal cluster-level statistics that exceeds the observed maximum or minimum original cluster-level test statistics. Because this method uses maxima, it intrinsically corrected for multiple comparisons in time and space. In each patient, HEP signals computed separately in synchronous and asynchronous conditions in the 0–600 ms post R-peak time window was submitted to the cluster based permutation *t*-test. Similar permutation tests were applied for comparing mean ITC values between synchronous and asynchronous stroking conditions (Fig. 7). For that, condition labels of single trial phase values were randomly shuffled and ITC was computed using these shuffled data, repeatedly 1000 times. Then, a permutation *P*-value was obtained as the proportion of differences of mean ITC between 2 conditions from shuffled data that exceed the original mean ITC difference.

To further confirm the results of our correlation analysis between ITC and power across recording sites (Fig. 3C), we applied a Bayesian approach (Liang et al. 2008; Rouder et al. 2009). We computed the inverse Bayes Factors (i.e., JZS Bayes factor) for those correlation analyses with the assumption that values larger than 3 would support the null-hypothesis, whereas values smaller than 1/3 would indicate evidence for the alternative hypothesis.

Results

Experiment-1: Neural Sources and Mechanisms of HEPs

In Experiment-1, we investigated the neural sources of HEPs and the underlying mechanisms of HEP generation. We started out by grand-averaging ITC of HEPs across all 474 bipolar derivations obtained from the 8 patients (Fig. 1). This was done to determine the time and frequency samples showing significant enhancement of ITC without any a priori assumption. We found that ITC significantly increased after the R-peak onset (Fig. 3A; permutation test in each time–frequency sample, FDR corrected $P < 0.005$). Strongest ITC enhancement was observed in a 100–250 ms post R-peak time window and in a frequency range from 4 to 7 Hz (Fig. 3A; white inset). We then checked whether these results were due to a single outlier (e.g., one dominant patient). For that, we repeated the same ITC analysis 8 times with 7 patients, leaving out one different patient each time. We found significant clusters of enhanced ITC in all 7 repetitions of analysis (permutation test, FDR corrected $P < 0.01$); this analysis always found the strongest effects in the time (100–250 ms) and frequency (4–7 Hz) ranges indicated by the white inset in Figure 3A. This control analysis thus confirms that the results were not driven by a single patient.

Similar analysis was conducted for the spectral power over the 474 bipolar derivations, which did not reveal any significant enhancement of spectral power using the same statistical procedures applied to ITC (Fig. 3B; permutation test, all FDR corrected $P > 0.05$). This suggests that neural responses to heartbeats are associated with the modulations of phases of ongoing neural activities, rather than enhancement of spectral power.

Next, we further tested the relationship between ITC and power across all bipolar derivations. To this aim, for each recording site, we computed the mean ITC and mean spectral power using the time and frequency samples that showed significant enhancement of ITC (i.e., time–frequency samples within the black contour lines in Fig. 3A). For each patient, these mean values at each recording site were transformed

into Z-scores using the mean and the SD obtained across all recorded electrodes. Pearson's r between ITC and power across all bipolar derivations from all patients revealed no significant correlation (Fig. 3C; Pearson's r across all 474 bipolar derivations: $r = 0.057$, $P = 0.22$). Additional analysis using a Bayesian approach confirmed the absence of a correlation between ITC and power across all recording sites (inverse Bayes factor = 30.14). When restricting the same correlation analysis to the recording sites that showed significant enhancement of ITC (see below), we again could not find any significant correlation between ITC and power (Pearson's r across 48 recording sites: $r = 0.086$, $P = 0.56$; inverse Bayes factor = 7.45). These results reveal that HEPs are (1) associated with heartbeat-induced phase concentration, (2) not associated with any heartbeat-induced enhancement of power, and (3) that there is no correlation between ITC and power, suggesting that the phase reset mechanism, rather than the additive evoked mechanism, might underlie the generation of HEP (see Discussion).

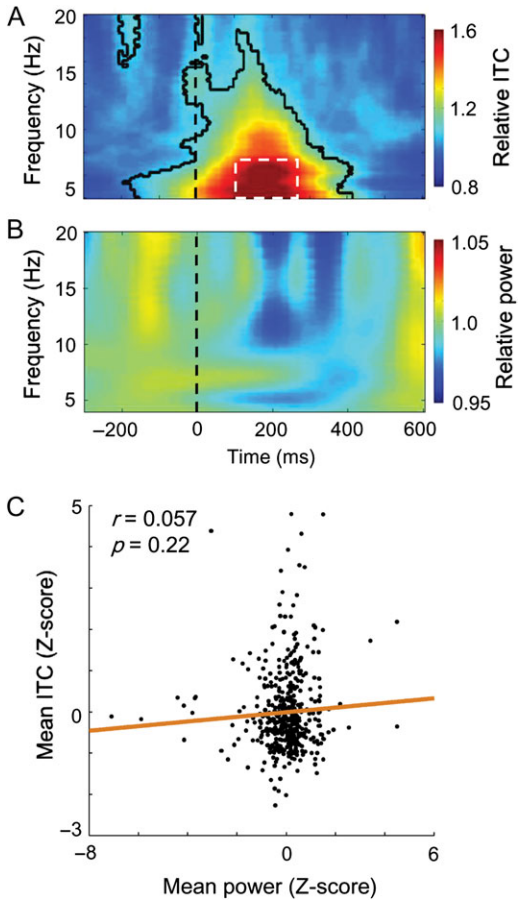

Figure 3. Grand-averaged ITC and spectral power of HEPs across all 474 bipolar derivations from 8 patients, and correlation between them. (*A*) Grand averaged ITC over all bipolar derivations. Black contour lines indicate significant samples (FDR corrected $P < 0.005$). (*B*) Grand averaged spectral power over all bipolar derivations. Baseline correction (−300 to −100 ms regarding the R-peak onset) was applied for both ITC and power. (*C*) No significant correlation was observed between ITC and power across all bipolar derivations ($P = 0.22$, inverse Bayes factor = 30.14).

Next, we analyzed where the recording sites, which showed the significant ITC enhancements, were localized. We computed the mean ITC values within the significant cluster observed in the grand-averaged result (which are indicated in Fig. 3A) for each bipolar derivation, and obtained corresponding P-values using permutation tests (see Materials and Methods). This analysis revealed that 48 bipolar derivations (10% of all analyzed bipolar sites) showed significant ITC enhancement (Fig. 4; permutation test, FDR corrected $P < 0.05$).

Among the 48 significant bipolar derivations, 33% (16/48) were located in the insula or the operculum (Fig. 5; Table. 1). Heartbeat-locked intracranial EEG directly recorded at the insula and operculum showed a negligible influence of the CFA. Interestingly, some adjacent bipolar derivations showed polarity reversal (Fig. 5A) and heartbeat induced ITC enhancement, suggesting that the actual sources might be located between these 2 bipolar derivations (Lachaux et al. 2003). More specifically, as these 2 bipolar derivations (e.g., A1–A2 and A2–A3) were obtained from 3 contiguous contacts (e.g., A1, A2, A3), the location of middle contact (e.g., A2; middle point between green and red dots in Fig. 5A; MNI coordinate: −34, −5, 4) would likely be closest to the actual source. As shown in Figure 5B, results of 3 consecutive recording sites from P-2 showed another interesting pattern which suggests that the HEP might consist of 2 distinct components: a lower frequency component (4–7 Hz) and a higher frequency component (8–20 Hz). Among these three recording sites, the higher frequency component (8–20 Hz) was most prominent in the 200–400 ms time window (see the blue HEP waveform and corresponding ITC result in Fig. 5B) at the most superficial recording site (Fig. 5B, indicated by a blue dot). This higher frequency component progressively decreased (see the green and red HEP waveforms and corresponding ITC results in Fig. 5B) at adjacent, but deeper recording sites (Fig. 5B, indicated by green and red dots). The opposite pattern was observed in the lower frequency band (4–7 Hz): the deepest

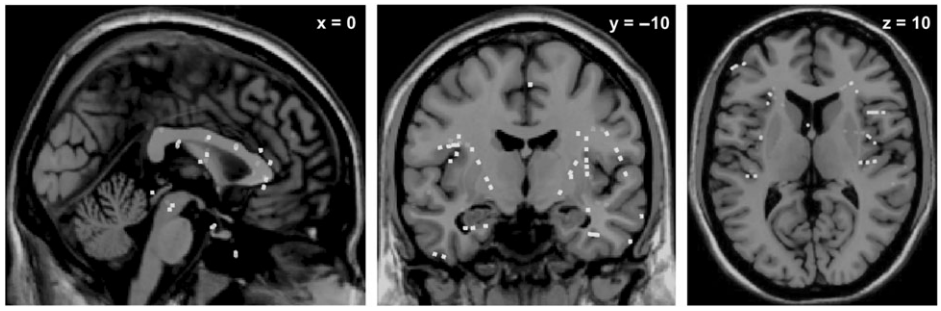

Figure 4. Locations of bipolar derivations that showed significant ITC enhancement (FDR corrected $P < 0.05$) in 3D MNI space. A third of significant bipolar derivations (16 among 48 recording sites) were located at the insula and operculum. Note that locations are in 3D MNI space, and not located on the surface of MRI slice shown (thus, recording sites behind the depicted MRI slice are marked with faded color). See Supplementary Table 2 for the MNI coordinates of each recording site and corresponding FDR corrected P-values.

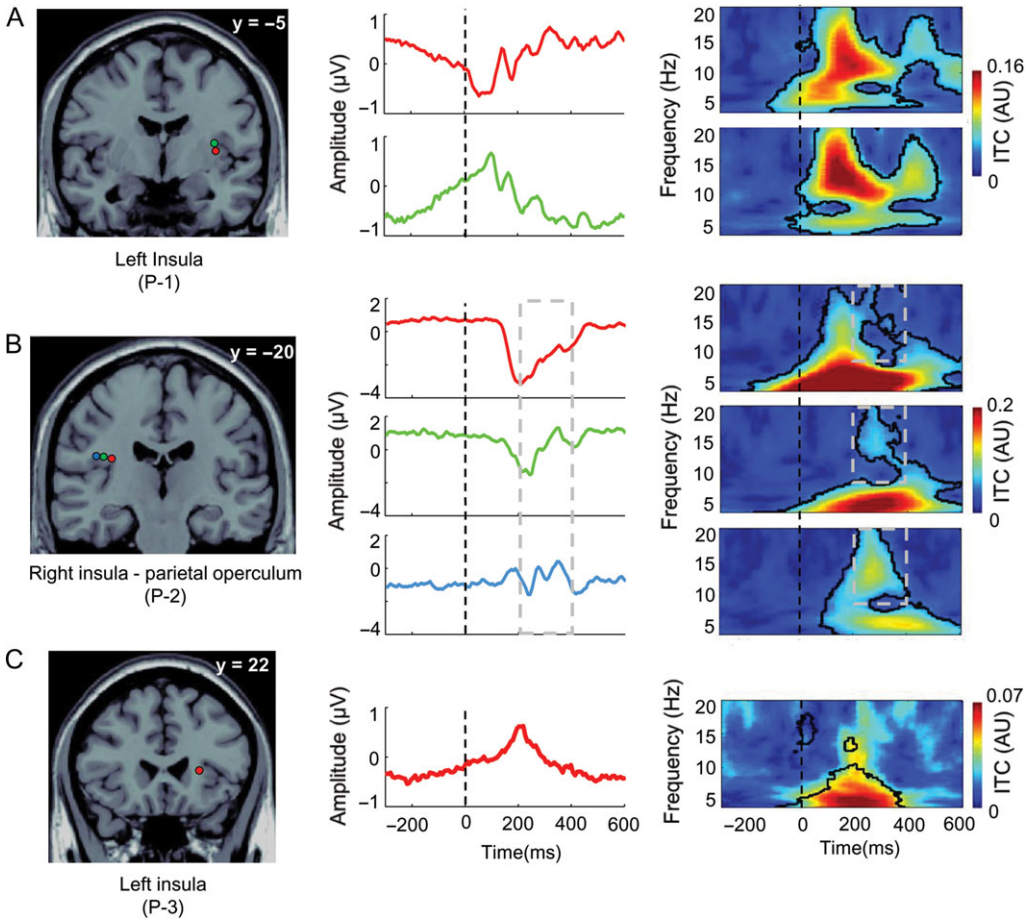

Figure 5. Exemplar HEP waveforms and their corresponding ITC results at the insula and operculum from 3 different patients. (*A*) Results from P-1. Significant recording sites were located at the left posterior insular cortex (left). Two HEP waveforms from adjacent bipolar derivations showed polarity reversal phenomena (middle) and transient enhancement of ITC was observed in both recording sites (right). (*B*) Results from P-2. Significant recording sites were located at the right insula and operculum (left). Transient enhancement of ITC was observed (right) in all three bipolar signals (middle). The recording site indicated by a red and a blue dot showed dominant low frequency and high frequency activations, respectively. Gray dotted boxes indicate the 200–400 ms time window (middle) and 8–20 Hz frequency band (right) that progressive modulation of higher frequency components was observed across three recording sites. (*C*) Results from P-3. A significant bipolar derivation was located at the left insula (left). Transient enhancement of ITC was observed (right). Note that at a single recording site level, baseline correction was not applied to show the original ITC values. Black contour lines indicate significant samples (FDR corrected $P < 0.05$).

Table 1 Number of significant bipolar derivations and all recording sites, sorted by brain regions (FDR corrected $P < 0.05$).

Region	Number of significant bipolar derivations/all bipolar derivations
Insular cortex	11/33
Central operculum cortex	3/9
Frontal operculum cortex	1/15
Parietal operculum cortex	1/5
Inferior frontal gyrus	4/29
Frontal pole	4/41
Middle frontal gyrus	1/29
Temporal fusiform cortex	5/23
Middle temporal gyrus	3/39
Temporal pole	3/32
Amygdala	3/16
Hippocampus	1/11
Parahippocampal gyrus	1/22
Putamen	1/3
Supramarginal gyrus	1/6
Supplementary motor cortex	1/2
White matter	4/41

recording site showed the strongest lower frequency component that progressively decreased at the more superficial recording sites. This result suggests that lower frequency and higher frequency component of HEP might originate from different neural sources. Other recording sites with significant effects were found in widespread regions including the inferior frontal gyrus, amygdala, temporal fusiform cortex, middle temporal gyrus, frontal pole, and temporal pole (Table 1).

We also checked whether the latency or frequency of observed ITC enhancement depends on the length of cardiac cycles (i.e., IBIs). For that we divided all R-peak locked single trials into short-IBI (mean IBI = 0.7417, SD = 0.0723) and long-IBI trials (mean IBI = 0.8601, SD = 0.0885) using a median split, and computed ITC of short-IBI and long-IBI trials separately, in each 48 recording sites that showed significant ITC enhancement. The latency and frequency of the strongest ITC enhancement, averaged over all 48 recording sites, was similar in short-IBI and long-IBI trials (i.e., 100–250 ms and 4–7 Hz range; see Supplementary Fig. 1). Mean ITC enhancement between short-IBI and long-IBI trials was not significantly different (permutation test on mean ITC values over 100–250 ms and 4–7 Hz range across 48 recording sites, $P = 0.55$).

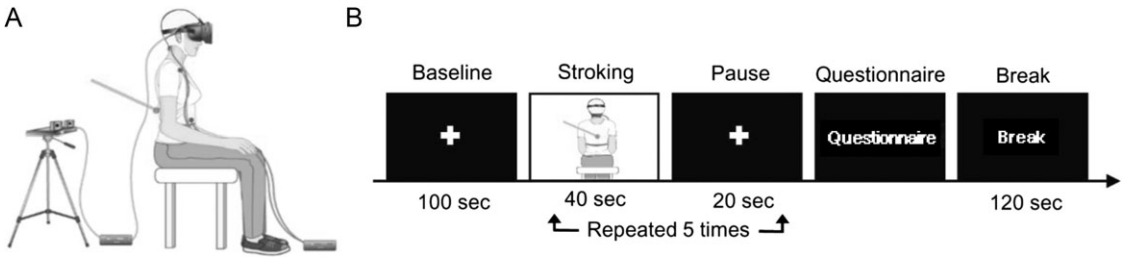

Figure 6. Experimental set-up and procedure in Experiment-2. (*A*) Intracranial EEG and ECG signals were simultaneously recorded while patient's backs were stroked either synchronously or asynchronously with a virtually presented image of their own back via head-mounted display. Red dots indicate the location of ECG electrodes. (*B*) Time course of a block. After 5 stroking-pause repetitions, patients were instructed to respond to the questionnaire. Adopted from Park et al. (2016).

Experiment-2: HEPs in the Insula and Operculum Reflect Modulation of Self-identification

In Experiment-2, 4 patients (P-1, P-2, P-5, P-8) implanted with depth electrodes involving the insula or the operculum additionally performed the FBI task (Fig. 6), while intracranial EEG signals were recorded (Lenggenhager et al. 2007; Ionta et al. 2011; Blanke et al. 2015; Park et al. 2016). Subjective responses varied in 2 patients who reported a stronger sense of self-identification with the avatar during the synchronous condition compared with the asynchronous condition (P-1, Sync: 7, Async: 1; P-5, Sync: 7, Async: 1).

In patient P-1, 13 bipolar derivations from 2 depth electrodes that contained at least one insular or opercular contact were analyzed. In Experiment-1, 5 bipolar derivations located in the insula (out of 13) showed significantly enhanced ITC. Of these, only one bipolar derivation located in left insular cortex showed a differential HEP amplitude between synchronous and asynchronous stroking conditions (Fig. 7*A*; green dot) in the 217–367 ms post R-peak time window (cluster-based permutation *t*-test, cluster-level $P = 0.01$). No differential HEP amplitude changes were observed during the baseline or during the pause period (Fig. 7*A*; both cluster-level $P > 0.25$). Next, we checked whether such differential HEP waveforms were associated with differential modulation of ITC between synchronous and asynchronous stroking conditions. Although significantly enhanced ITC was observed in both conditions (Fig. 7*A*, right-top, permutation test, FDR-corrected $P < 0.05$; significant samples are indicated by black contour lines), stronger ITC enhancement was observed in the asynchronous versus synchronous stroking condition in the same time window for which we observed differential HEP waveforms (Fig. 7*A*, right bottom; permutation test on mean ITC in the 217–367 ms, and 4–20 Hz range, $P = 0.024$). Such a mean ITC difference was not observed during the no-stroking periods (i.e., baseline and pause periods; see Fig. 6*B*) between 2 conditions ($P = 0.194$). Mean IBI during stroking periods, using no-stroking periods for baseline correction, between synchronous and asynchronous conditions were not different (2 sample *t*-test, $t_{(385)} = 1.539$, $P = 0.125$).

In patient P-5, 7 bipolar derivations from 2 depth electrodes were analyzed. Although none of these 7 recording sites showed ITC enhancement in Experiment-1, one bipolar derivation located in the left insular cortex (Fig. 7*B*; green dot) showed a differential modulation of HEP amplitude between synchronous and asynchronous stroking conditions (Fig. 7*B*; cluster-level $P = 0.032$) in the 402–512 ms post R-peak time window. Again such a differential HEP modulation was not observed during the baseline or pause period (both cluster-level $P > 0.55$). In this patient, enhanced ITC was observed neither during synchronous nor asynchronous stroking conditions (Fig. 7*B*, right-top; all FDR corrected $P > 0.05$). Also, no differential ITC were observed in the time window for which differential HEP waveforms was observed during the stroking periods or no-stroking periods (permutation test on mean ITC in the 402–512 ms, and 4–20 Hz range, both $P > 0.14$). Mean IBI during stroking periods between synchronous and asynchronous conditions were not different (two sample *t*-test, $t_{(489)} = -0.884$, $P = 0.377$). Importantly, in both patients there was no influence of CFA, excluding the possibility that differential HEP might reflect the difference in CFA.

Next, we checked whether this selective and differential activation between conditions was specifically associated with the heartbeat. For this, we conducted the same HEP analysis repeatedly (100 times) using surrogate R-peaks, which had the same mean IBI and variability as original R-peaks but were shifted randomly in time (Park et al. 2014, 2016; Babo-Rebelo, Richter, et al. 2016). This analysis revealed no cluster statistic (i.e., sum of *t*-values within the largest cluster) that was equal to or greater than the one initially obtained from the HEP with real R-peaks in both P-1 and P-5 (Fig. 7*A*,*B*; both Monte-Carlo $P = 0.01$), confirming that the differential HEP effect was time-locked to the heartbeat.

Finally, we analyzed HEPs in 2 other patients (P-2, P-8) who reported strong levels of self-identification with the avatar, but of equal strength between the synchronous and asynchronous conditions (P-2, Sync: 7, Async: 7; P-8, Sync: 7, Async: 7). In patient P-2, 7 bipolar derivations from a depth electrode shaft that contained insular electrode contacts were analyzed. Although ITC enhancement was observed in three out of 7 bipolar derivations (see Fig. 5*B*) in Experiment-1, none of them showed a differential modulation of HEP amplitude between synchronous and asynchronous conditions during the stroking or baseline or pause periods (all cluster-level $P > 0.1$). In patient P-8, 14 bipolar derivations from 2 depth electrode shafts that contained at least one insular or operculum recording sites were analyzed. None of these recording sites showed ITC enhancement in Experiment-1, nor a differential HEP amplitude between synchronous and asynchronous conditions was observed during the stroking or baseline or pause periods (all cluster-level $P > 0.3$). These results support our hypothesis that differential modulations of HEPs in the insula and operculum are associated with stroking dependent modulations of self-identification.

Discussion

Despite recent growing interest in HEPs as a neural marker of cardiac-related cortical processing in diverse cognitive functions, their fundamental properties are yet to be understood. Here, we found that neural responses to heartbeats can be

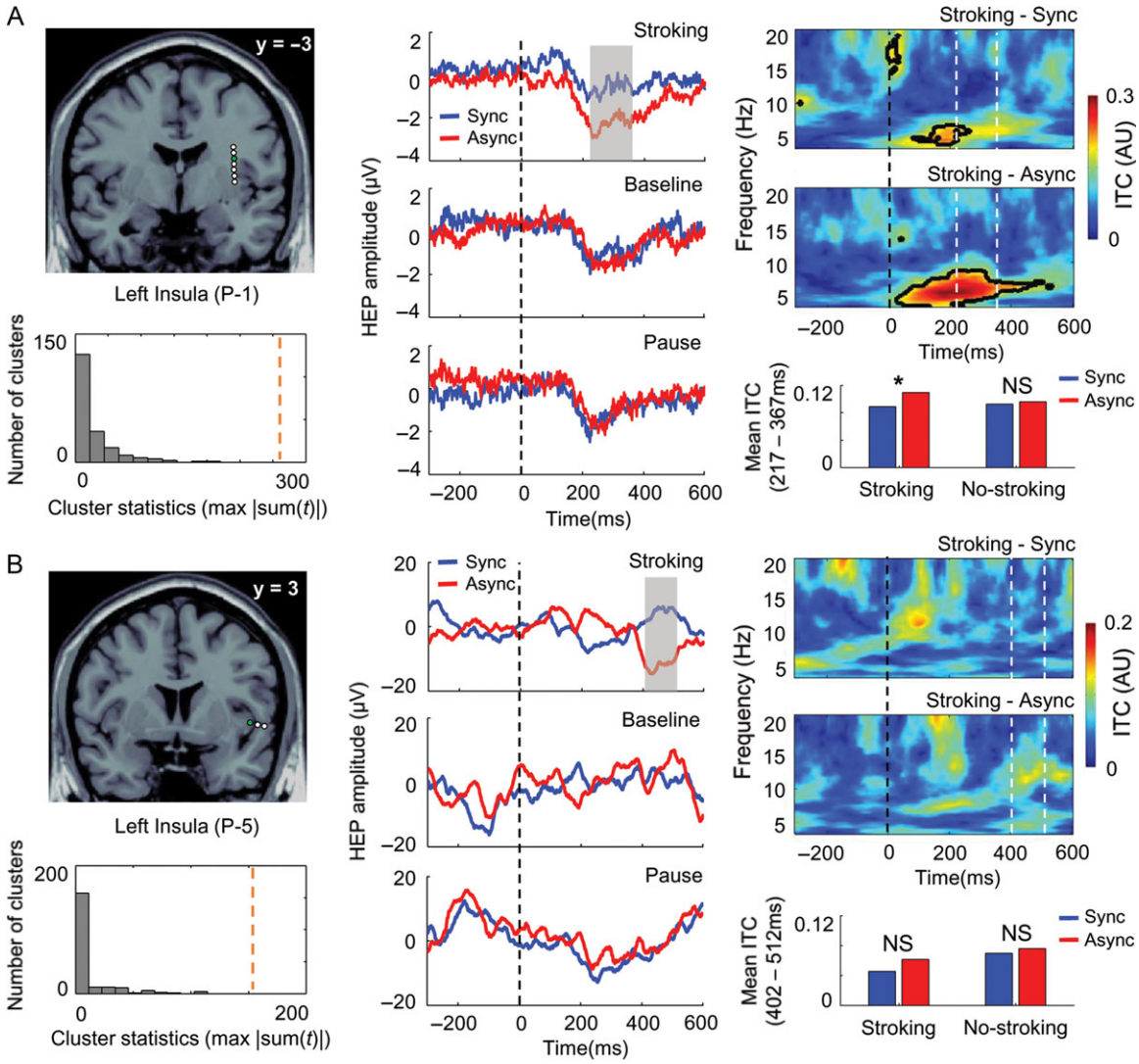

Figure 7. Differential modulation of HEPs between synchronous and asynchronous visuo-tactile stimulation during the FBI experiment. (*A*) Results from P-1. Among 7 bipolar derivations shown (black circles), one (green dot) located at the left insula showed differential HEP modulations between 2 conditions (left-top). Differential modulations of HEPs were observed during the stroking (cluster level $P = 0.01$; middle-top), but not during the baseline (middle-middle) or pause (middle-bottom) period at the recording site marked in green in the left-top. Histogram of the maximal cluster statistics obtained from surrogate heartbeats (left-bottom). Although significantly enhanced ITC was observed in both Stoking-Sync and Stroking-Async conditions (right-top; FDR-corrected $P < 0.05$), stronger ITC was observed in the Stroking-Async condition during the time window (217–367 ms) that differential HEP waveforms were observed (right-bottom; permutation test, $P = 0.024$). Such differential ITC modulation was not observed during the no-stroking period (right-bottom; $P = 0.194$). (*B*) Results from P-5. Among 3 bipolar derivations shown (black circles), one (green dot) located at the left insula showed differential HEP modulations between 2 conditions (left-top). Differential modulations of HEPs were observed during the stroking (cluster level $P = 0.032$; middle-top), but not during the baseline (middle-middle) or pause (middle-bottom) period at the recording site marked in green in the left-top. Histogram of the maximal cluster statistics obtained from surrogate heartbeats (left-bottom). Significantly enhanced ITC was observed neither in Stroking-Sync nor Stroking-Async conditions (right-top, FDR-corrected $P > 0.05$). No differential ITC modulations between Sync and Async conditions were observed in the time window (402–512 ms) that differential HEP waveforms were observed (right-bottom; permutation test, both $P > 0.14$). Yellow dotted lines indicate the cluster statistic obtained from original heartbeats. The shaded area highlights the time window in which a significant difference of the HEP amplitude was observed. White dotted vertical lines in the time–frequency plots indicate the time window in which a significant difference of the HEP amplitude was observed. Black contour lines indicate significant samples (FDR-corrected $P < 0.05$).

recorded mainly in insular and opercular regions, although we also found HEPs in other regions distributed across the brain including the amygdala and fronto-temporal cortex. Increased phase concentration of HEPs was not accompanied by spectral power changes, and there was no correlation between both measurements, suggesting that a phase resetting mechanism underlies HEP generation. These findings provide novel and solid evidence about the HEP's electrophysiological mechanism and the anatomical location of its neural sources.

The Insular and Operculum are Primary Neural Sources of the HEP

The major proportion of recording sites that showed significantly increased HEPs as based on heartbeat-induced phase concentration was observed in 2 main cortical regions: the insula (i.e., anterior, posterior) and operculum (i.e., frontal, central, posterior). The insula has been proposed as the primary cortical projection site of interoceptive signals (Craig 2003, 2009; Critchley and Harrison 2013; Damasio and Carvalho 2013;

Park and Tallon-Baudry 2014). Thus, visceral afferents reach the insula either through a cranial nerve pathway (i.e., vagus nerve) or spinal relay, mainly targeting the nucleus of the solitary tract, parabrachial nucleus, and ventromedial nucleus of the thalamus (Saper 2002; Craig 2003). Indeed, using intracranial EEG, a recent single patient study reported that HEP-like waveforms can be observed at the insula (Canales-Johnson et al. 2015). In that study, which primarily focused on surface EEG data, HEP-like waveforms were reported at 2 recording sites (in the anterior insula and orbitofrontal cortex); importantly, although a polarity reversal between these 2 recording sites was shown, the authors did not support their HEP result by statistical or quantitative analysis. In the present study, by analyzing intracranial EEG data from 474 recording sites in 8 patients, along with rigorous statistical procedures, we provide solid evidence for the role of the insula in the neural processing of cardiac signals, compatible with its prominent role in processing of interoceptive signals. Another study reported intracranial HEPs (using cortical grid electrodes), but this time in the primary somatosensory cortex (Kern et al. 2013) by showing consistent HEP-like waveforms across 3 patients out of 6, but without statistical analysis. Indeed, it has been shown that both the insula and somatosensory cortex are critical for the heartbeat-related processing (Khalsa et al. 2009). Khalsa and colleagues showed that a rare neurological patient with severe bilateral insular damage had normal cardiac sensation, whereas cardiac sensations disappeared when his chest skin was anaesthetized, suggesting the insular and somatosensory cortices independently process cardiac afferent signals (Khalsa et al. 2009). Accordingly, a recent brain stimulation study showed that transcranial magnetic stimulation (TMS) over the insula and somatosensory cortex resulted in differential effects on interoceptive processing (Pollatos et al. 2016), although it is debatable whether TMS can effectively stimulate deep brain areas like the insula (Zangen et al. 2005). Additionally, fMRI studies suggested the importance of somatosensory activations, commonly coactivated with the insula, in interoception (Critchley et al. 2004; Pollatos et al. 2007; Hassanpour et al. 2016). Together with these previous data, the present results are compatible with previous proposals that cardiac interoceptive pathways consist of multifaceted subcomponents including a sensory component mediated through the skin and primary somatosensory regions as well as an interoceptive component mainly processed in the insula (Khalsa et al. 2009; Pollatos et al. 2016).

Beyond the insula and operculum, we found evidence of HEPs in more distributed cortical areas such as the amygdala, inferior frontal gyrus, frontal pole, temporal fusiform cortex, middle temporal gyrus, and the temporal pole. A prominent account of interoception proposes that the insula and anterior cingulate cortex might be the sole cortical substrates representing interoceptive afferents and their conscious awareness (Craig 2003, 2009, 2011). However, the present HEP results fit better with accounts that have proposed that interoceptive signals are processed in widely distributed cortical areas including, next to the insula, also the amygdala, the cingulate cortex, and the somatosensory cortex (Pollatos et al. 2007, 2016; Khalsa et al. 2009, 2016; Critchley and Harrison 2013; Park and Tallon-Baudry 2014; Hassanpour et al. 2016; Adolfi et al. 2017). Furthermore, we note that such HEP modulations were observed not only in viscerosensory regions (e.g., insula, operculum), but also in putative visceromotor regions (e.g., amygdala, putamen, supplementary motor cortex). This finding is in accordance with a recently suggested account of interoceptive predictive coding proposing that the interoceptive system is composed of visceromotor and viscerosensory cortices generating interoceptive prediction and prediction-error signals, respectively (Barrett and Simmons 2015). Further work using simultaneous EEG-fMRI recordings would be necessary to understand the differences in interoceptive processing between the different regions of this large network and how such signals are integrated.

We also note limitations regarding the present electrode locations that are inherent to intracranial EEG data. First, although we were fortunate to have the possibility to record from multiple intracranial electrodes in the insula or operculum, which are rarely explored in epileptic patients (Burns et al. 2014), other proposed cortical targets of visceral afferents, such as the anterior cingulate cortex, could not be systematically investigated, and many cortical regions remained undersampled due to the clinical nature of the electrode implantation. Second, electrode locations were also inhomogeneous across patients and may have been undersampled within the insula or the operculum. For instance, in Experiment-2, although no recorded bipolar signals at the insula or operculum showed differential HEP modulations between synchronous and asynchronous conditions in patients without illusory effects, there remains the possibility that other parts of the insula or operculum might have shown differential HEP modulations between conditions (see below). Due to these reasons, we decided to not further differentiate between subparts of the insula (i.e., anterior or posterior) and the operculum (i.e., frontal, central, posterior) in interpreting our results, and considered the insula and the operculum as a contiguous interoceptive processing system (Craig 2003, 2009). Also, although the right insula has been proposed as a more dominant cortical source of interoceptive processing (Craig 2003), such lateralization of the insular processing could not be examined in this study because of abovementioned limitations (i.e., the low sample size and the clinically determined uneven hemispheric implantations). In addition, the methods applied in Experiment-2 were correlative in nature. Thus a follow-up TMS study would be able to reveal the causal link between HEP in the insula and bodily self-consciousness, preferably using the H-Coil that is designed to target deep brain regions (Zangen et al. 2005).

Relationship Between HEPs and Other Heart-cycle Related Physiological Changes

When investigating HEPs, it is critical to demonstrate that observed heartbeat-related effects reflect genuine neural activity rather than heart cycle-related artifacts such as CFA or PA (Dirlich et al. 1997; Kern et al. 2013). First, it is evident that our results cannot reflect mere CFA. In accordance with a previous intracranial HEP data (Kern et al. 2013), we observed a negligible impact of CFA on the waveforms of the heartbeat-locked intracranial EEG signals (Figs 2, 5 and 7). Furthermore, peak phase concentration was observed about 200 ms after the R-peak onset, rather than around the R-peak itself, arguing against that the ITC enhancement in the present data was caused by CFA. Presumably, bipolar referencing applied in the current study further attenuated such CFA in the data. In the present study, we moreover focused on dissociating the HEP from PA. Up to now, exact origins of PA as observed in heartbeat locked intracranial EEG signals are unknown. For instance, a previous study examined the relationship between the PA amplitude and the location of subdural blood vessels (i.e., the vena anastomotica inferior), but did not find any meaningful pattern, and suggested that epidural vessels, pulsatile cerebrospinal fluid, and cardiac cycle related brain motion may be potential

sources of PA (Kern et al. 2013). In the present study, we expected that bipolar referencing might be able to effectively remove such PA originating from common and remote sources, but that was not the case. For removing such PA components, we made 2 important assumptions based on known properties of PA and HEPs; namely that the frequency bands of PA and the pulse rate would be matched (i.e., lower than 2 Hz), and that the phase concentration of HEPs after the R-peak would increase compared with the pre-R-peak period. On the basis of both assumptions, we applied a time–frequency approach and removed low frequency components below 4 Hz. In addition, we applied a baseline correction for the statistical analysis to find HEP components whose ITC values were greater than those at the prestimulus interval.

Although this method could effectively remove the slower components (<4 Hz) of heart cycle related artifacts such as PA, the possibility still remains that there could be some mechanical artifact whose frequency is higher than 4 Hz. For instance, we cannot exclude that the observed HEPs are associated with above 4 Hz vascular activities in local blood vessels. Indeed, this is potential limitation of all intracranial HEP studies, as no study has measured and removed all heart cycle related vascular activities that could artifactually affect intracranial EEG signals. We propose that the evidence of the phase-resetting mechanism (i.e., increased phase concentration without spectral power enhancement) is probably one of the strongest arguments supporting the finding that observed HEP effect does not reflect pure mechanical artifacts, compared with previous studies relying on visual inspection to distinguish between HEP and PA (Kern et al. 2013). We argue that if our results reflect artifacts associated with the mechanical movement of blood vessels (e.g., dilation and constriction of vessels), they should rather be associated with a modulation of power or amplitude (i.e., due to the gradual impedance changes associated with the mechanical pulsation, see Luck 2014) than the phase of the single trial waveforms. Of note, the relationship between vascular and neural activities is complex and not well understood yet. On the one hand, it is known that neural activity increases local blood flow, which is a fundamental principle of functional magnetic resonance imaging (O'Herron et al. 2016). On the other hand, a recent animal study showed that changes in cerebral blood flow also impacts resting neuronal activity in the brain (Kim et al. 2016), suggesting that there is a two-way communication between blood vessels and neurons in the brain. In our data, a "−300 to −100 ms" time window was used as a baseline and the strongest phase-resetting effects were observed around 100–250 ms time window after the R-peak, which roughly correspond to the diastole and systole phase, respectively, suggesting that increased vascular activities during the systole phase could have induced HEP modulation through the phase-resetting mechanism. In addition, we observed similar ITC enhancement in short-IBI and long-IBI trials, indicating that HEP is time-locked to the onset of preceding heartbeat rather than a preparation of the next heartbeat (Park et al. 2014). Taken together, our results suggest that the observed enhancement of ITC reflects modulations of neural activities time-locked to heartbeats rather than heart-cycle related artifacts such as CFA or PA. Future research, for instance using invasive techniques in animals, should investigate (1) the interplay between cardiac afferent signals (e.g., stroke volume, blood pressure, sympathetic/parasympathetic nervous system responses) and neural responses to heartbeats, and (2) how such cardiac signals are transmitted to cortical areas.

Phase-Resetting Underlies HEP Generation

Our phase and spectral power analyses of HEPs suggest that a phase-resetting mechanism, rather than an additive evoked (potential) mechanism, underlies HEP generation. Several criteria have been proposed to distinguish ERPs (e.g., visual- and auditory evoked potentials) caused by phase-resetting and evoked mechanisms (for a review see Sauseng et al. 2007), and evidence supporting either the phase reset (Makeig et al. 2002; Rizzuto et al. 2003; Lakatos et al. 2013) or the evoked model (Shah et al. 2004; Mazaheri and Jensen 2006; Rousselet et al. 2007) have been reported. In the present study, we applied the simple and well-accepted criteria for distinguishing the phase-reset and the evoked model (Fell et al. 2004; Fuentemilla et al. 2006): evidence of stimulus-induced phase concentration without accompanying enhancement of spectral power supports the phase-reset model, whereas increased spectral power, regardless of the result of phase analysis, supports the evoked mechanism. Enhancement of phase concentration is necessary but not sufficient for phase-resetting of the HEP, as "evoked" responses with fixed latency can also result in a similar phase concentration of the HEP. Thus, only phase concentration without power enhancement is compatible with the phase resetting mechanism. In accordance with these predictions of the phase-reset model, we observed increased ITC around 200 ms after the R-peak, mainly in a frequency range from 4 to 7 Hz, without accompanying spectral power enhancement. Moreover, correlation analysis between ITC and spectral power has been argued to provide additional criteria for differentiating phase-resetting from evoked mechanisms (Lopour et al. 2013). Accordingly, we observed no correlation between ITC and spectral power across recording sites, thus confirming that phase concentration was not accompanied by spectral power changes. Taken together, our results suggest that heartbeats might provide internal temporal triggers to the brain and generate heartbeat "evoked" potentials by resetting the phase of ongoing oscillations, rather than by adding evoked responses.

What could be the potential functional roles of observed ITC modulations recorded at rest? First, it has been shown that heartbeats are consciously perceived about 200–300 ms after the R-peak onset (Brener and Kluvitse 1988), and heartbeat perception performance varies substantially across individuals (Khalsa and Lapidus 2016). Thus, it is possible that observed modulations of ITC around 250 ms post R-peak in Experiment-1 are associated with the patients' ability to detect heartbeats, which is in accordance with previous studies reported a positive correlation between the HEP amplitude and heartbeat perception score across individuals (Pollatos and Schandry 2004). Second, several recent studies have shown that the cardiac cycle (e.g., phase or frequency) impacts emotional appraisal (Gray et al. 2012; Garfinkel et al. 2014), visual awareness (Salomon et al. 2016), memory encoding (Garfinkel et al. 2013), somatosensory processing (Edwards et al. 2009; Gray et al. 2009), body ownership (Aspell et al. 2013; Suzuki et al. 2013; Sel et al. 2016), and more recently social bias (Azevedo et al. 2017). Our findings could provide a potential explanation of such influence of the cardiac cycle on behavior. For instance, Garfinkel and colleagues observed that emotional appraisal of fearful stimuli was enhanced during the systole phase (i.e., around 300 ms after the R-peak), which was accompanied by increased amygdala BOLD activation, compared with the diastole phase (i.e., around R-peak onset; see Garfinkel et al. 2014). Accordingly, in Experiment-1, we also observed increased ITC around the systole phase at the subset of amygdala electrodes, compared with the

baseline period which corresponds to the diastole phase. Presumably, enhanced phase-resetting at the amygdala in the systole phase could have facilitated such emotional processing of fearful stimuli. Future work is need to directly test this proposal.

HEPs in the Insula Reflect Bodily Self-consciousness

In a subset of patients, we also investigated whether local brain activity in the insula and the operculum is associated with experimentally-induced changes in bodily self-consciousness. We report that modulations of HEPs directly recorded at the insula were associated with alteration of bodily self-consciousness (e.g., self-identification) as experimentally induced by the FBI paradigm. In one patient (P-1), such differential HEP waveforms (in the 217–367 ms time window) between 2 conditions were accompanied by different modulations of ITC enhancement, indicating that the modulation (i.e., strength) of phase-resetting observed in Experiment-1 is also involved in the present effects in bodily self-consciousness. However, differential HEP waveforms observed in another patient (P-5, in the 402–512 ms time window) were not associated with such ITC modulations, although a very weak trend was observed ($P = 0.147$). These data suggest that neural responses to heartbeats consist of (1) phase-locked HEP components reflecting primary cortical sources of cardiac afferents, and (2) non or weakly phase-locked HEP components probably reflecting secondary processing of signals from primary sources processing heartbeat related signals. This interpretation is in accordance with previous findings that showed sensory evoked brain activity (e.g., gamma band oscillations) consist of phase locked and non-phase locked components which occur in earlier (e.g., <300 ms) and later (e.g., >300 ms) time windows, respectively (Tallon-Baudry and Bertrand 1999).

In a previous scalp EEG study from our group that used the same behavioral task (Park et al. 2016), the cortical sources of differential HEPs were observed in the bilateral posterior cingulate cortex and the left insula; however, the relatively small cluster at the insula did not survive stringent corrections for multiple comparisons when using surface EEG data. In the present study, using intracranial EEG with high spatial resolution, we revealed that differential heartbeat-locked local field potentials recorded at the insula were associated with the differential subjective feelings of self-identification in 2 patients. Relatedly, a recent intracranial EEG study found that the amplitude of HEPs in the insula is parametrically associated with self-relatedness of spontaneous thoughts in a single patient (Babo-Rebelo, Wolpert, et al. 2016). Although the experimental approaches used in the present and Babo-Rebelo and colleagues' study are very different, they are complementary in suggesting an implication of cardiac signals and self-related processing in the insula: we experimentally altered the sense of bodily self-consciousness by modulating visuo-tactile multisensory stimulation, whereas Babo-Rebelo and colleagues measured the degree of self-relatedness during spontaneous thought fluctuations (Babo-Rebelo, Richter, et al. 2016; Babo-Rebelo, Wolpert, et al. 2016). Together with recent neurological data about abnormal states of self-identification induced by abnormal integration of cardio-visual signals (Heydrich and Blanke 2013; Ronchi et al. 2015) and brain imaging data showing cardiac effects on visual consciousness (Park et al. 2014; Salomon et al. 2016), these data provide converging evidence supporting the claim that the neural processing of interoceptive signals in the insula is important for self-consciousness (Craig 2009; Critchley and Harrison 2013; Seth 2013; Park and Tallon-Baudry 2014; Blanke et al. 2015).

In conclusion, we demonstrated here that the insula and operculum are primary neural sources of the HEP among the recorded brain regions, and that a phase resetting might be the key brain mechanism for HEP generation. Our results provide novel and solid evidence on the fundamental properties of HEPs such as their neural distribution and underlying electrophysiological mechanisms. We further showed that HEPs directly recorded at the insula are associated with a modulation of the sense of self-consciousness, confirming and extending our previous scalp EEG study (Park et al. 2016). Together with recent studies (Park et al. 2014, 2016; Canales-Johnson et al. 2015; Babo-Rebelo, Richter, et al. 2016; Babo-Rebelo, Wolpert, et al. 2016; Sel et al. 2016), our results also suggest that HEPs are reliable neural marker for brain–body interactions and the role of such interactions in cognitive and emotional processes, in particular the subjective aspect of conscious experiences including perceptual awareness and self-consciousness.

Supplementary Material

Supplementary material is available at *Cerebral Cortex* online.

Funding

This work was supported by the Fondation Bertarelli to H.D.P. and O.B., the Swiss National Science Foundation to M.S. (no. SNF 163398).

Notes

We thank Alexandre Belhassen, Guillaume Mollard, Rafael Rolli for technical supports, Jeroen van Baar, Pierre Mégevand for useful discussion. *Conflict of Interest*: The authors declare no competing financial interests.

References

Adolfi F, Couto B, Richter F, Decety J, Lopez J, Sigman M, Manes F, Ibanez A. 2017. Convergence of interoception, emotion, and social cognition: a twofold fMRI meta-analysis and lesion approach. Cortex. 88:124–142.

Aspell JE, Heydrich L, Marillier G, Lavanchy T, Herbelin B, Blanke O. 2013. Turning body and self inside out: visualized heartbeats alter bodily self-consciousness and tactile perception. Psychol Sci. 24:2445–2453.

Azevedo RT, Garfinkel SN, Critchley HD, Tsakiris M. 2017. Cardiac afferent activity modulates the expression of racial stereotypes. Nat Commun. 8:13854.

Babo-Rebelo M, Richter CG, Tallon-Baudry C. 2016a. Neural responses to heartbeats in the default network encode the self in spontaneous thoughts. J Neurosci. 36:7829–7840.

Babo-Rebelo M, Wolpert N, Adam C, Hasboun D, Tallon-Baudry C. 2016b. Is the cardiac monitoring function related to the self in both the default network and right anterior insula? Philos Trans R Soc Lond B Biol Sci. 371:20160004.

Barrett LF, Simmons WK. 2015. Interoceptive predictions in the brain. Nat Rev Neurosci. 16:419–429.

Benjamini Y, Hochberg Y. 1995. Controlling the false discovery rate – a practical and powerful approach to multiple testing. J R Stat Soc B Methodol. 57:289–300.

Blanke O, Mohr C, Michel CM, Pascual-Leone A, Brugger P, Seeck M, Landis T, Thut G. 2005. Linking out-of-body experience and self processing to mental own-body imagery at the temporoparietal junction. J Neurosci. 25:550–557.

Blanke O, Slater M, Serino A. 2015. Behavioral, neural, and computational principles of bodily self-consciousness. Neuron. 88: 145–166.

Brener J, Kluvitse C. 1988. Heartbeat detection: judgments of the simultaneity of external stimuli and heartbeats. Psychophysiology. 25:554–561.

Brunet D, Murray MM, Michel CM. 2011. Spatiotemporal analysis of multichannel EEG: CARTOOL. Comput Intell Neurosci. 2011:813870.

Burns SP, Santaniello S, Yaffe RB, Jouny CC, Crone NE, Bergey GK, Anderson WS, Sarma SV. 2014. Network dynamics of the brain and influence of the epileptic seizure onset zone. Proc Natl Acad Sci USA. 111:E5321–E5330.

Canales-Johnson A, Silva C, Huepe D, Rivera-Rei A, Noreika V, Garcia MD, Silva W, Ciraolo C, Vaucheret E, Sedeno L, et al. 2015. Auditory feedback differentially modulates behavioral and neural markers of objective and subjective performance when tapping to your heartbeat. Cereb Cortex. 25:4490–4503.

Cechetto DF, Calaresu FR. 1985. Central pathways relaying cardiovascular afferent information to amygdala. Am J Physiol. 248:R38–R45.

Christoff K, Cosmelli D, Legrand D, Thompson E. 2011. Specifying the self for cognitive neuroscience. Trends Cogn Sci. 15:104–112.

Craig AD. 2003. Interoception: the sense of the physiological condition of the body. Curr Opin Neurobiol. 13:500–505.

Craig AD. 2009. How do you feel–now? The anterior insula and human awareness. Nat Rev Neurosci. 10:59–70.

Craig AD. 2011. Significance of the insula for the evolution of human awareness of feelings from the body. Ann NY Acad Sci. 1225:72–82.

Critchley HD, Harrison NA. 2013. Visceral influences on brain and behavior. Neuron. 77:624–638.

Critchley HD, Wiens S, Rotshtein P, Ohman A, Dolan RJ. 2004. Neural systems supporting interoceptive awareness. Nat Neurosci. 7:189–195.

Damasio A, Carvalho GB. 2013. The nature of feelings: evolutionary and neurobiological origins. Nat Rev Neurosci. 14:143–152.

Dirlich G, Vogl L, Plaschke M, Strian F. 1997. Cardiac field effects on the EEG. Electroencephalogr Clin Neurophysiol. 102: 307–315.

Dum RP, Levinthal DJ, Strick PL. 2009. The spinothalamic system targets motor and sensory areas in the cerebral cortex of monkeys. J Neurosci. 29:14223–14235.

Edwards L, Ring C, McIntyre D, Winer JB, Martin U. 2009. Sensory detection thresholds are modulated across the cardiac cycle: evidence that cutaneous sensibility is greatest for systolic stimulation. Psychophysiology. 46:252–256.

Fell J, Dietl T, Grunwald T, Kurthen M, Klaver P, Trautner P, Schaller C, Elger CE, Fernandez G. 2004. Neural bases of cognitive ERPs: more than phase reset. J Cogn Neurosci. 16: 1595–1604.

Fuentemilla L, Marco-Pallares J, Grau C. 2006. Modulation of spectral power and of phase resetting of EEG contributes differentially to the generation of auditory event-related potentials. Neuroimage. 30:909–916.

Fukushima H, Terasawa Y, Umeda S. 2011. Association between interoception and empathy: evidence from heartbeat-evoked brain potential. Int J Psychophysiol. 79:259–265.

Garfinkel SN, Barrett AB, Minati L, Dolan RJ, Seth AK, Critchley HD. 2013. What the heart forgets: cardiac timing influences memory for words and is modulated by metacognition and interoceptive sensitivity. Psychophysiology. 50:505–512.

Garfinkel SN, Critchley HD. 2016. Threat and the body: how the heart supports fear processing. Trends Cogn Sci. 20:34–46.

Garfinkel SN, Minati L, Gray MA, Seth AK, Dolan RJ, Critchley HD. 2014. Fear from the heart: sensitivity to fear stimuli depends on individual heartbeats. J Neurosci. 34:6573–6582.

Gray MA, Beacher FD, Minati L, Nagai Y, Kemp AH, Harrison NA, Critchley HD. 2012. Emotional appraisal is influenced by cardiac afferent information. Emotion. 12:180–191.

Gray MA, Rylander K, Harrison NA, Wallin BG, Critchley HD. 2009. Following one's heart: cardiac rhythms gate central initiation of sympathetic reflexes. J Neurosci. 29:1817–1825.

Gray MA, Taggart P, Sutton PM, Groves D, Holdright DR, Bradbury D, Brull D, Critchley HD. 2007. A cortical potential reflecting cardiac function. Proc Natl Acad Sci USA. 104: 6818–6823.

Groppe DM, Urbach TP, Kutas M. 2011. Mass univariate analysis of event-related brain potentials/fields I: a critical tutorial review. Psychophysiology. 48:1711–1725.

Hassanpour MS, Yan LR, Wang DJJ, Lapidus RC, Arevian AC, Simmons WK, Feusner JD, Khalsa SS. 2016. How the heart speaks to the brain: neural activity during cardiorespiratory interoceptive stimulation. Philos Trans R Soc B Biol Sci. 371: 20160017.

Heydrich L, Blanke O. 2013. Distinct illusory own-body perceptions caused by damage to posterior insula and extrastriate cortex. Brain. 136:790–803.

Ionta S, Heydrich L, Lenggenhager B, Mouthon M, Fornari E, Chapuis D, Gassert R, Blanke O. 2011. Multisensory mechanisms in temporo-parietal cortex support self-location and first-person perspective. Neuron. 70:363–374.

Kern M, Aertsen A, Schulze-Bonhage A, Ball T. 2013. Heart cycle-related effects on event-related potentials, spectral power changes, and connectivity patterns in the human ECoG. Neuroimage. 81:178–190.

Khalsa SS, Feinstein JS, Li W, Feusner JD, Adolphs R, Hurlemann R. 2016. Panic anxiety in humans with bilateral amygdala lesions: pharmacological induction via cardiorespiratory interoceptive pathways. J Neurosci. 36:3559–3566.

Khalsa SS, Lapidus RC. 2016. Can interoception improve the pragmatic search for biomarkers in psychiatry? Front Psychiatry. 7:121.

Khalsa SS, Rudrauf D, Feinstein JS, Tranel D. 2009. The pathways of interoceptive awareness. Nat Neurosci. 12:1494–1496.

Kim KJ, Ramiro Diaz J, Iddings JA, Filosa JA. 2016. Vasculo-neuronal coupling: retrograde vascular communication to brain neurons. J Neurosci. 36:12624–12639.

Lachaux JP, Rudrauf D, Kahane P. 2003. Intracranial EEG and human brain mapping. J Physiol Paris. 97:613–628.

Lakatos P, Musacchia G, O'Connel MN, Falchier AY, Javitt DC, Schroeder CE. 2013. The spectrotemporal filter mechanism of auditory selective attention. Neuron. 77:750–761.

Lechinger J, Heib DP, Gruber W, Schabus M, Klimesch W. 2015. Heartbeat-related EEG amplitude and phase modulations from wakefulness to deep sleep: Interactions with sleep spindles and slow oscillations. Psychophysiology. 52:1441–1450.

Lenggenhager B, Tadi T, Metzinger T, Blanke O. 2007. Video ergo sum: manipulating bodily self-consciousness. Science. 317:1096–1099.

Liang F, Paulo R, Molina G, Clyde MA, Berger JO. 2008. Mixtures of g priors for Bayesian variable selection. J Am Stat Assoc. 103:410–423.

Lopour BA, Tavassoli A, Fried I, Ringach DL. 2013. Coding of information in the phase of local field potentials within human medial temporal lobe. Neuron. 79:594–606.

Luck SJ. 2014. An introduction to the event-related potential technique. 2nd ed. Cambridge (MA): The MIT Press.

Makeig S, Westerfield M, Jung TP, Enghoff S, Townsend J, Courchesne E, Sejnowski TJ. 2002. Dynamic brain sources of visual evoked responses. Science. 295:690–694.

Makris N, Goldstein JM, Kennedy D, Hodge SM, Caviness VS, Faraone SV, Tsuang MT, Seidman LJ. 2006. Decreased volume of left and total anterior insular lobule in schizophrenia. Schizophr Res. 83:155–171.

Maris E, Oostenveld R. 2007. Nonparametric statistical testing of EEG- and MEG-data. J Neurosci Methods. 164:177–190.

Mazaheri A, Jensen O. 2006. Posterior alpha activity is not phase-reset by visual stimuli. Proc Natl Acad Sci USA. 103: 2948–2952.

Montoya P, Schandry R, Muller A. 1993. Heartbeat evoked potentials (HEP): topography and influence of cardiac awareness and focus of attention. Electroencephalogr Clin Neurophysiol. 88:163–172.

Muller LE, Schulz A, Andermann M, Gabel A, Gescher DM, Spohn A, Herpertz SC, Bertsch K. 2015. Cortical representation of afferent bodily signals in borderline personality disorder: neural correlates and relationship to emotional dysregulation. JAMA Psychiatry. 72:1077–1086.

Norcia AM, Appelbaum LG, Ales JM, Cottereau BR, Rossion B. 2015. The steady-state visual evoked potential in vision research: A review. J Vis. 15:4.

O'Herron P, Chhatbar PY, Levy M, Shen Z, Schramm AE, Lu Z, Kara P. 2016. Neural correlates of single-vessel haemodynamic responses in vivo. Nature. 534:378–382.

Oostenveld R, Fries P, Maris E, Schoffelen JM. 2011. FieldTrip: open source software for advanced analysis of MEG, EEG, and invasive electrophysiological data. Comput Intell Neurosci. 2011:156869.

Park HD, Correia S, Ducorps A, Tallon-Baudry C. 2014. Spontaneous fluctuations in neural responses to heartbeats predict visual detection. Nat Neurosci. 17:612–618.

Park HD, Bernasconi F, Bello-Ruiz J, Pfeiffer C, Salomon R, Blanke O. 2016. Transient modulations of neural responses to heartbeats covary with bodily self-consciousness. J Neurosci. 36:8453–8460.

Park HD, Tallon-Baudry C. 2014. The neural subjective frame: from bodily signals to perceptual consciousness. Philos Trans R Soc Lond B Biol Sci. 369:20130208.

Pollatos O, Kirsch W, Schandry R. 2005. Brain structures involved in interoceptive awareness and cardioafferent signal processing: a dipole source localization study. Hum Brain Mapp. 26: 54–64.

Pollatos O, Herbert BM, Mai S, Kammer T. 2016. Changes in interoceptive processes following brain stimulation. Philos Trans R Soc Lond B Biol Sci. 371:20160016.

Pollatos O, Schandry R. 2004. Accuracy of heartbeat perception is reflected in the amplitude of the heartbeat-evoked brain potential. Psychophysiology. 41:476–482.

Pollatos O, Schandry R, Auer DP, Kaufmann C. 2007. Brain structures mediating cardiovascular arousal and interoceptive awareness. Brain Res. 1141:178–187.

Rizzuto DS, Madsen JR, Bromfield EB, Schulze-Bonhage A, Seelig D, Aschenbrenner-Scheibe R, Kahana MJ. 2003. Reset of human neocortical oscillations during a working memory task. Proc Natl Acad Sci USA. 100:7931–7936.

Roach BJ, Mathalon DH. 2008. Event-related EEG time-frequency analysis: an overview of measures and an analysis of early gamma band phase locking in schizophrenia. Schizophr Bull. 34:907–926.

Ronchi R, Bello-Ruiz J, Lukowska M, Herbelin B, Cabrilo I, Schaller K, Blanke O. 2015. Right insular damage decreases heartbeat awareness and alters cardio-visual effects on bodily self-consciousness. Neuropsychologia. 70:11–20.

Rouder JN, Speckman PL, Sun D, Morey RD, Iverson G. 2009. Bayesian t tests for accepting and rejecting the null hypothesis. Psychon Bull Rev. 16:225–237.

Rousselet GA, Husk JS, Bennett PJ, Sekuler AB. 2007. Single-trial EEG dynamics of object and face visual processing. Neuroimage. 36:843–862.

Salomon R, Ronchi R, Donz J, Bello-Ruiz J, Herbelin B, Martet R, Faivre N, Schaller K, Blanke O. 2016. The insula mediates access to awareness of visual stimuli presented synchronously to the heartbeat. J Neurosci. 36:5115–5127.

Saper CB. 2002. The central autonomic nervous system: conscious visceral perception and autonomic pattern generation. Annu Rev Neurosci. 25:433–469.

Sauseng P, Klimesch W, Gruber WR, Hanslmayr S, Freunberger R, Doppelmayr M. 2007. Are event-related potential components generated by phase resetting of brain oscillations? A critical discussion. Neuroscience. 146:1435–1444.

Schandry R, Sparrer B, Weitkunat R. 1986. From the heart to the brain: a study of heartbeat contingent scalp potentials. Int J Neurosci. 30:261–275.

Schulz A, Koster S, Beutel ME, Schachinger H, Vogele C, Rost S, Rauh M, Michal M. 2015. Altered patterns of heartbeat-evoked potentials in depersonalization/derealization disorder: neurophysiological evidence for impaired cortical representation of bodily signals. Psychosom Med. 77:506–516.

Sel A, Azevedo R, Tsakiris M. 2016. Heartfelt self: cardio-visual integration affects self-face recognition and interoceptive cortical processing. Cereb Cortex. 1–12. DOI: https://doi.org/10.1093/cercor/bhw296.

Seth AK. 2013. Interoceptive inference, emotion, and the embodied self. Trends Cogn Sci. 17:565–573.

Shah AS, Bressler SL, Knuth KH, Ding M, Mehta AD, Ulbert I, Schroeder CE. 2004. Neural dynamics and the fundamental mechanisms of event-related brain potentials. Cereb Cortex. 14:476–483.

Shao S, Shen K, Wilder-Smith EP, Li X. 2011. Effect of pain perception on the heartbeat evoked potential. Clin Neurophysiol. 122:1838–1845.

Sikes RW, Vogt LJ, Vogt BA. 2008. Distribution and properties of visceral nociceptive neurons in rabbit cingulate cortex. Pain. 135:160–174.

Suzuki K, Garfinkel SN, Critchley HD, Seth AK. 2013. Multisensory integration across exteroceptive and interoceptive domains modulates self-experience in the rubber-hand illusion. Neuropsychologia. 51:2909–2917.

Tadel F, Baillet S, Mosher JC, Pantazis D, Leahy RM. 2011. Brainstorm: a user-friendly application for MEG/EEG analysis. Comput Intell Neurosci. 2011:879716.

Tallon-Baudry C, Bertrand O. 1999. Oscillatory gamma activity in humans and its role in object representation. Trends Cogn Sci. 3:151–162.

Tallon-Baudry C, Bertrand O, Delpuech C, Pernier J. 1996. Stimulus specificity of phase-locked and non-phase-locked 40 Hz visual responses in human. J Neurosci. 16:4240–4249.

Terhaar J, Viola FC, Bar KJ, Debener S. 2012. Heartbeat evoked potentials mirror altered body perception in depressed patients. Clin Neurophysiol. 123:1950–1957.

Zangen A, Roth Y, Voller B, Hallett M. 2005. Transcranial magnetic stimulation of deep brain regions: evidence for efficacy of the H-coil. Clin Neurophysiol. 116:775–779.